# Supplementary Information

## Edible Temperature-Responsive-Adhesive Thermogalvanic Hydrogel for Self-Powered Multi-Sited Fatigue Monitoring

Xinru Zhang[a], Ning Li[a], Xiaojing Cui[b,c,*], Yu Li[a], Zhaosu Wang[a], Kai Zhuo[a], Hulin Zhang[a,*]

[a]College of Electronic Information and Optical Engineering, Taiyuan University of Technology, Taiyuan, 030024, China

[b]Shanxi Transportation Technology Research & Development Co., Ltd., Taiyuan 030032, China

[c]School of Physics and Information Engineering, Shanxi Normal University, Taiyuan 030031, China

*To whom correspondence should be addressed: 20210084@sxnu.edu.cn (X.C.); zhanghulin@tyut.edu.cn (H.Z.)

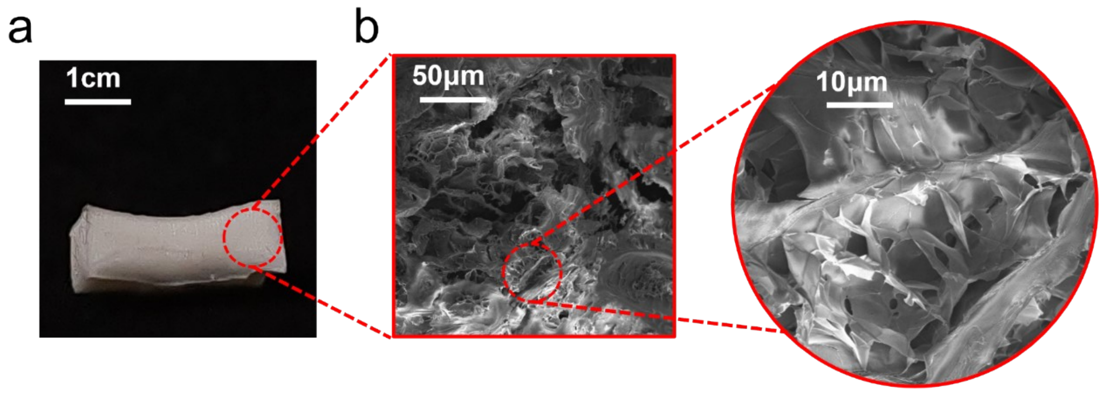


**Fig. S1** (a) Photo of the freeze-dried Gel/GL hydrogel. Scale bar (1 cm). (b) SEM images of the surface captured at various magnifications.

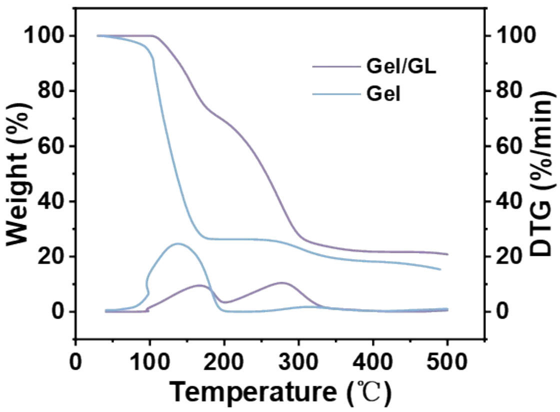


**Fig. S2** TG and DTG curves of the Gel/GL hydrogel.

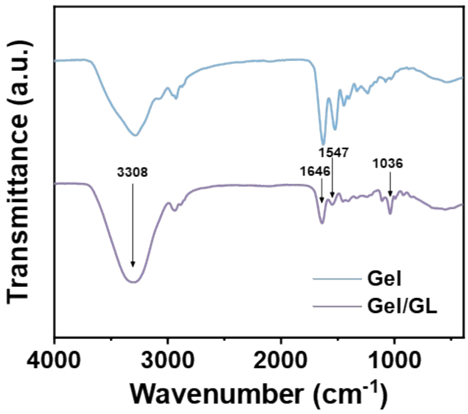


**Fig. S3** FTIR spectra of the Gel/GL hydrogel.

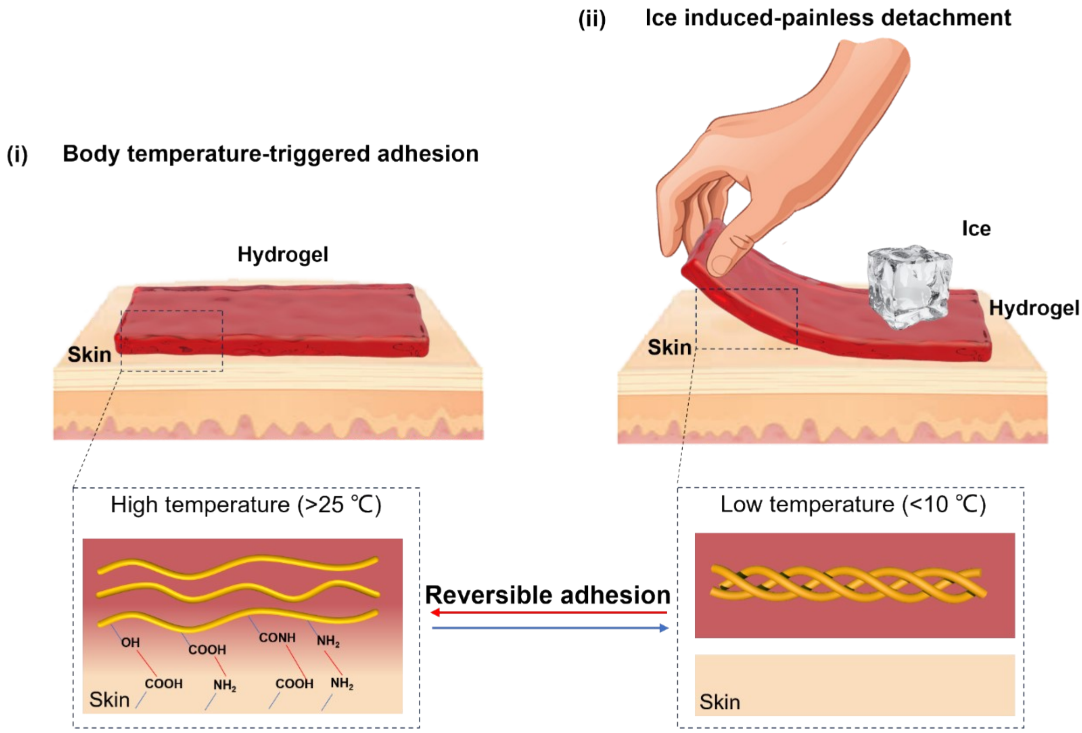


**Fig. S4** Schematic illustrations of the body temperature-triggered gentle adhesion and ice-cooling-induced painless detachment of the Gel/GL hydrogel.

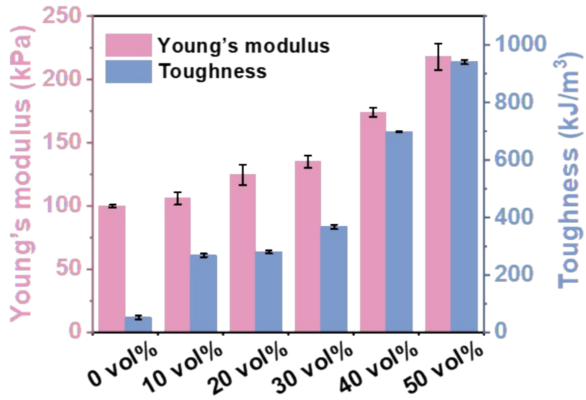


**Fig. S5** Comparison of the Young's modulus and toughness values of the Gel/GL hydrogel with different glycerol volume content.

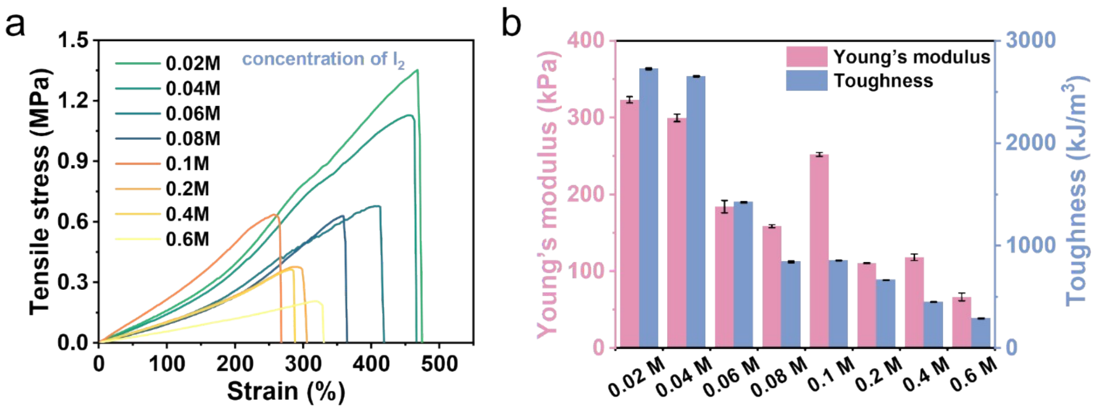


**Fig. S6** (a) The tensile stress-strain curves and (b) comparison of the Young's modulus and toughness values of the Gel/GL hydrogel with different $I_2$ content.

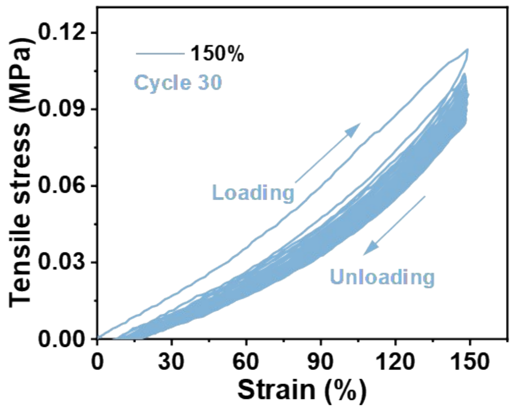


**Fig. S7** Continuous loading and unloading tests at 150% deformation.

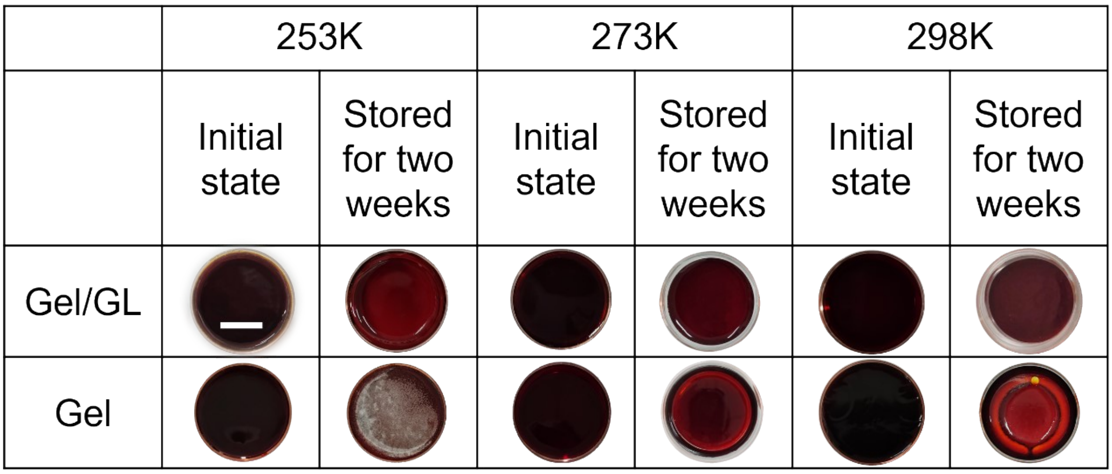


**Fig. S8** Photographs of the initial state of the hydrogel and the photos stored at different temperatures for two weeks. Scale bar (1 cm).

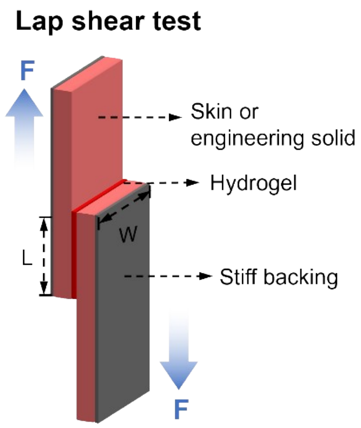


**Fig. S9** Schematic for the measurement of shear strength based on the standard lap shear test. *F* force, *W* width, *L* length.

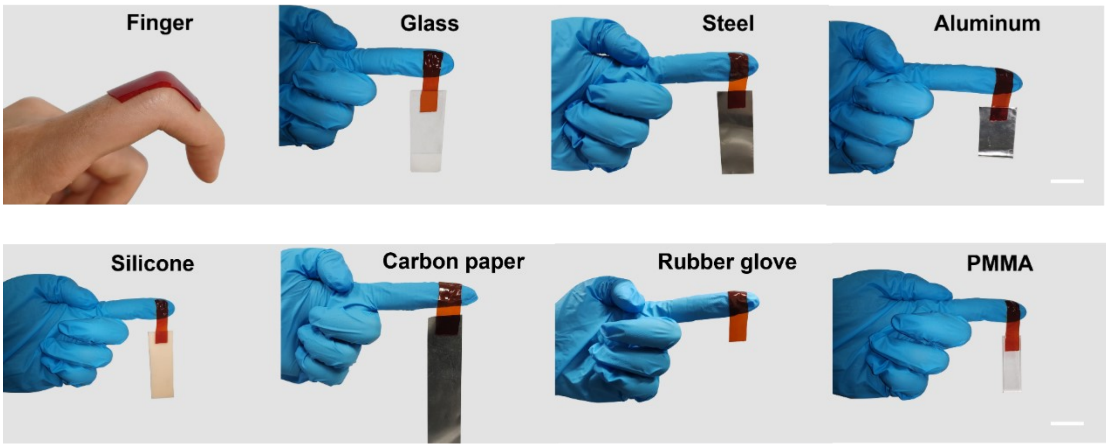


**Fig. S10** Photographs of adhesion of hydrogels to different materials. Scale bar (1 cm).

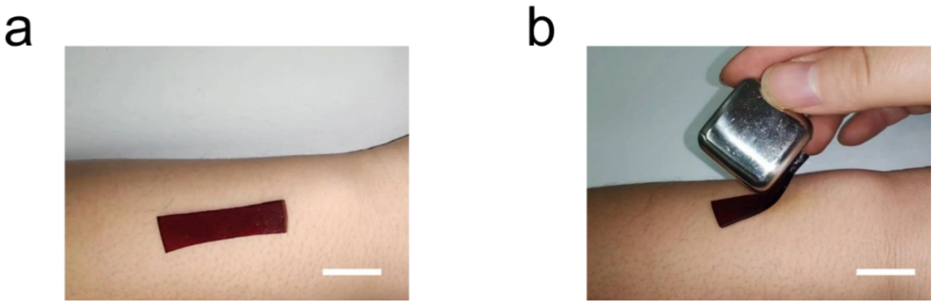


**Fig. S11** (a) Photographs of the hydrogel sticking to the skin and (b) removing after 10 seconds of freezing. Scale bar (1 cm).

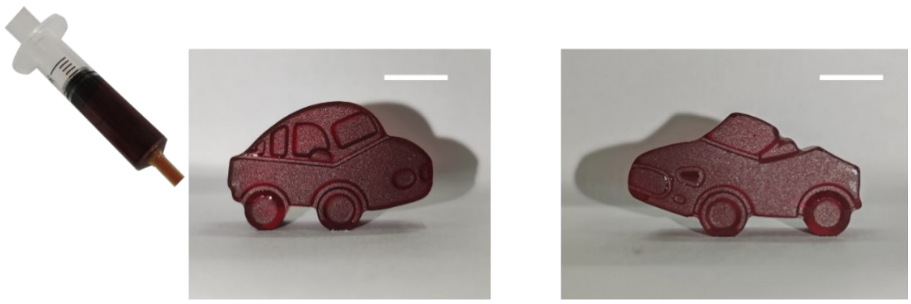

**Fig. S12** Photographs of the remodeling Gel/GL hydrogel with desired car shape. Scale bar (1 cm).

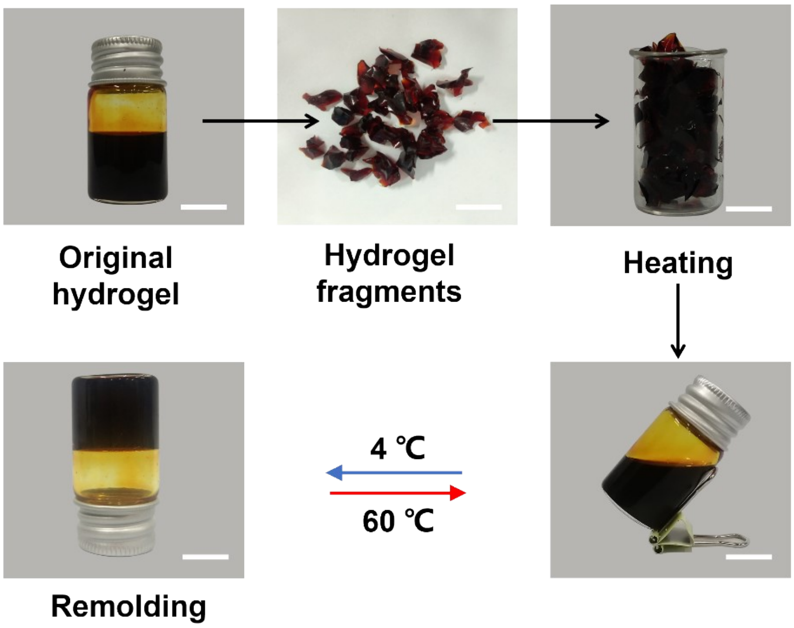


**Fig. S13** Reversible sol-gel transition of the Gel/GL hydrogel. Scale bar (1 cm).

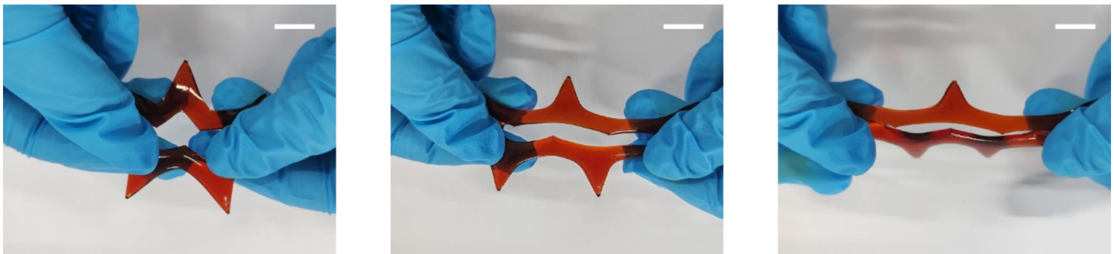

**Fig. S14** Photographs of the large stretching of remolded Gel/GL hydrogel. Scale bar (1 cm).

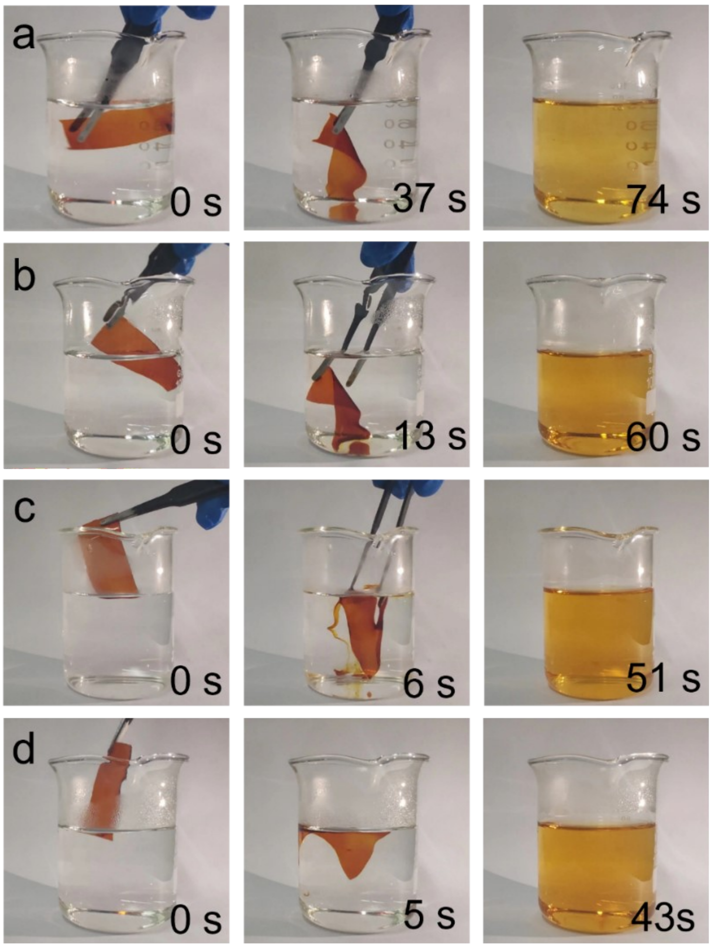


**Fig. S15** The dissolution of the Gel/GL hydrogel at 40 ℃ (a), 50 ℃ (b), 60 ℃ (c) and 70 ℃ (d). The softening and dissolution times of the hydrogels are 37 s, 13 s, 6 s, 5 s and 74 s, 60 s, 51 s, 43 s at temperatures of 40 ℃, 50 ℃, 60 ℃ and 70 ℃, respectively. Scale bar (1 cm).

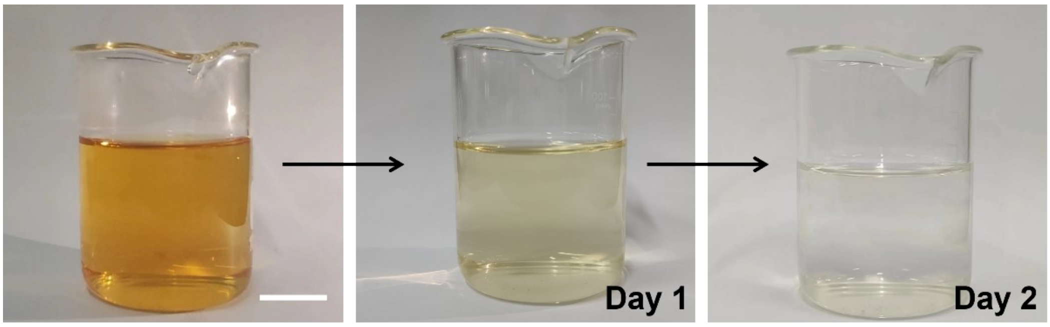


**Fig. S16** The changes of the Gel/GL hydrogel after dissolution stored at room temperature for two days. Scale bar (1 cm).

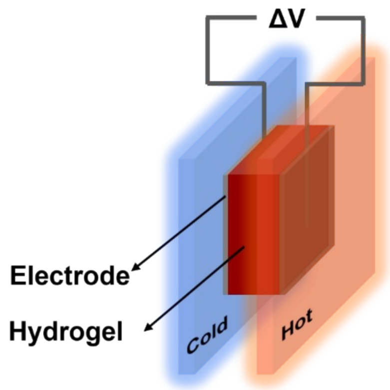


**Fig. S17** Schematic illustration of the Seebeck coefficient measurement setup.

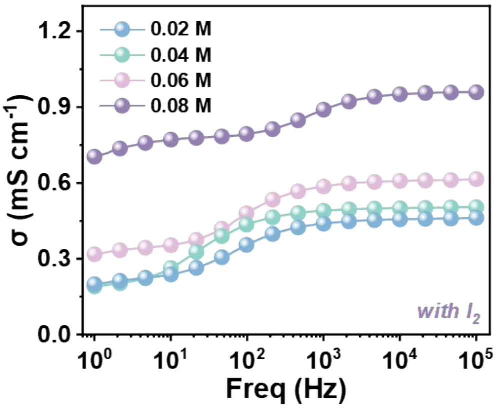


**Fig. S18** Frequency-dependent conductance of hydrogels with different doses of $I_2$.

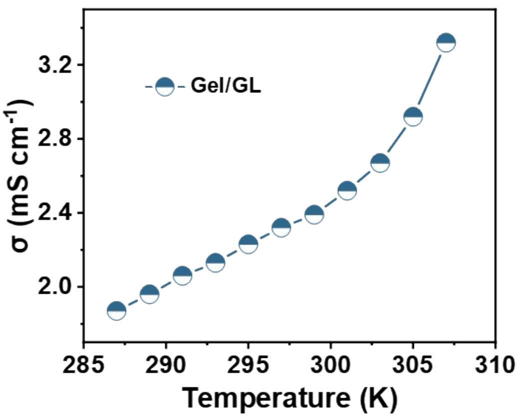


**Fig. S19** Variation of the electrical conductivity at different temperature gradients.

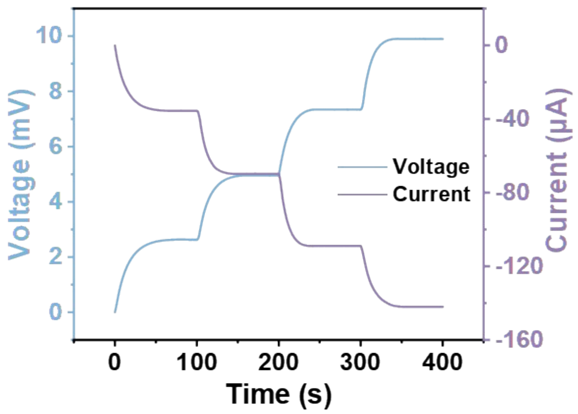


**Fig. S20** Corresponding output voltage and current response of the Gel/GL hydrogel under fixed temperature difference. The cold end is fixed at 273 K, and the temperature difference increment at the hot end is 5 K.

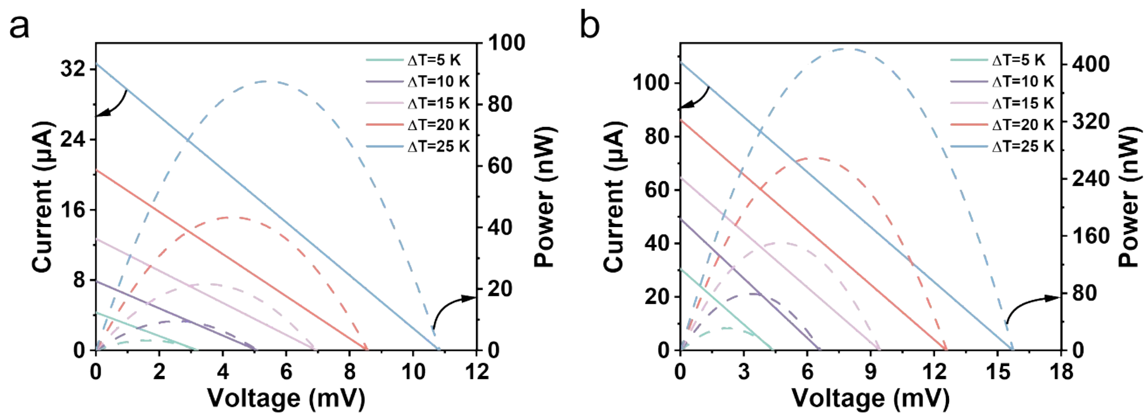


**Fig. S21** Current/power-voltage curves for the Gel/GL hydrogel with solvent/gelatin volume ratio of 4 (a) and 8 (b) at varying ΔT.

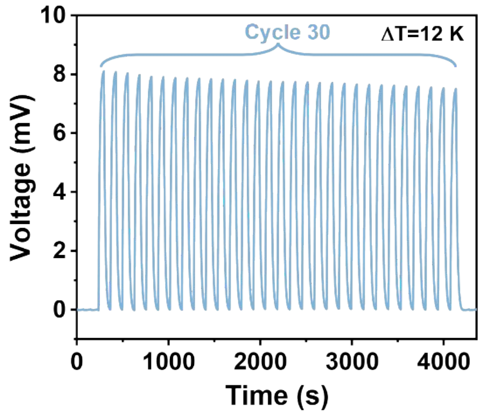


**Fig. S22** Thirty cycles of voltage output at a temperature difference of 12 K.

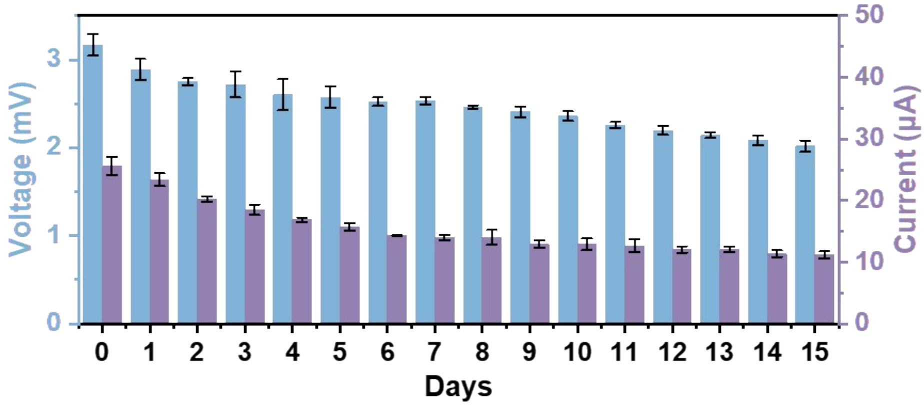


**Fig. S23** The voltage and current during 15 days of dehydration. ΔT = 5 K.

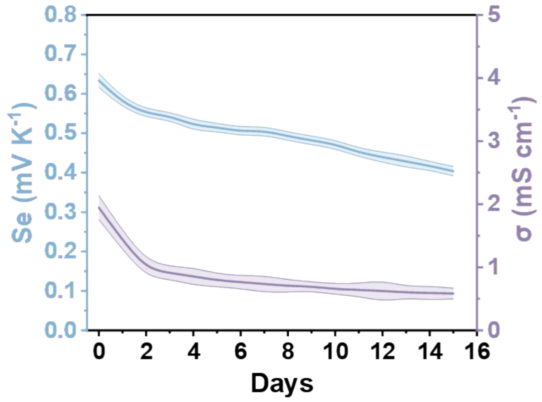


**Fig. S24** Se and σ variations for 15 days of dehydration.

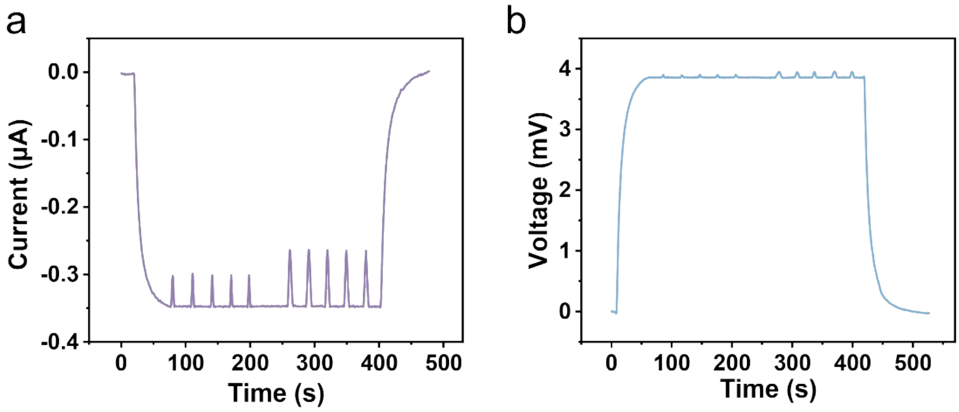


**Fig. S25** (a) Current-time and (b) voltage-time curves of the Gel/GL hydrogel being repeatedly stretched when $T_c$= 293 K and $T_h$= 298 K.

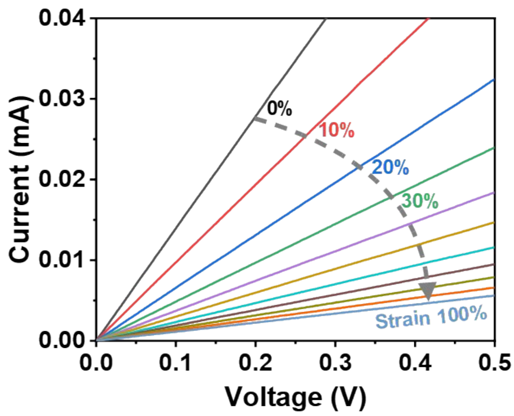


**Fig. S26** The current-voltage curves of the Gel/GL hydrogel at different stretched strains.

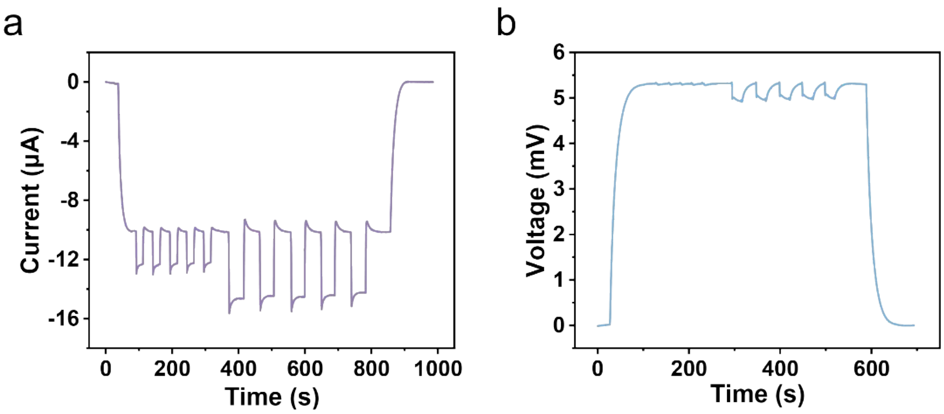


**Fig. S27** (a) Current-time and (b) voltage-time curves of the Gel/GL hydrogel being repeatedly pressed when $T_c$= 293 K and $T_h$= 298 K.

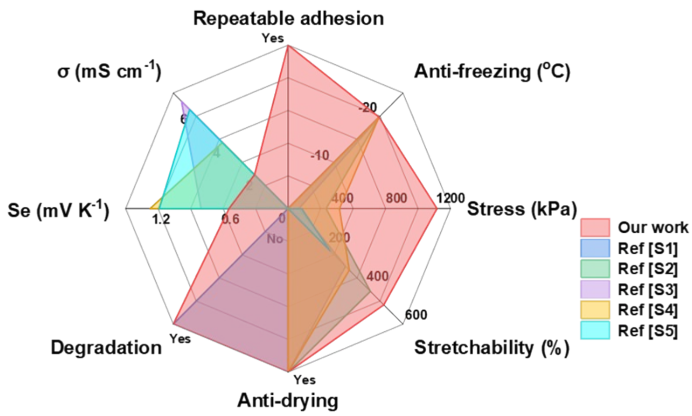


**Fig. S28** Comparison of the Gel/GL hydrogel with existing thermogalvanic gel in terms of the comprehensive performances.

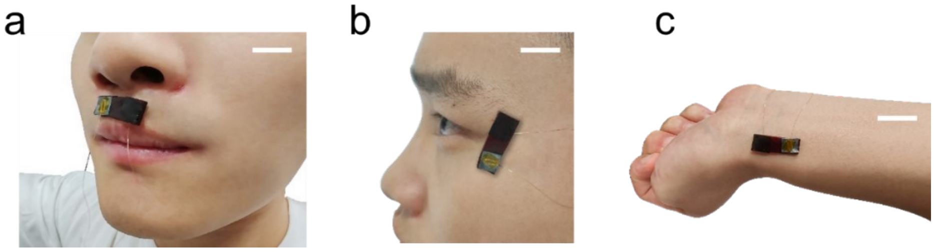


**Fig. S29** Photos of the hydrogel pasted in the corner of (a) the eye, (b) under the nose and (c) near the wrist. Scale bar (1 cm).

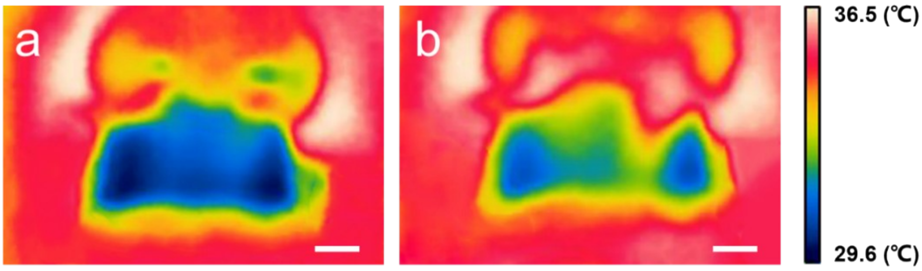


**Fig. S30** (a) The temperature distribution of the Gel/GL hydrogel during exhalation. (b) The temperature distribution of the Gel/GL hydrogel during inhalation. Scale bar (1 cm).

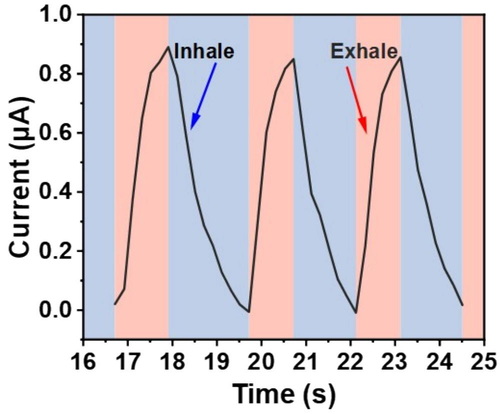


**Fig. S31** The amplified respiratory waveform.

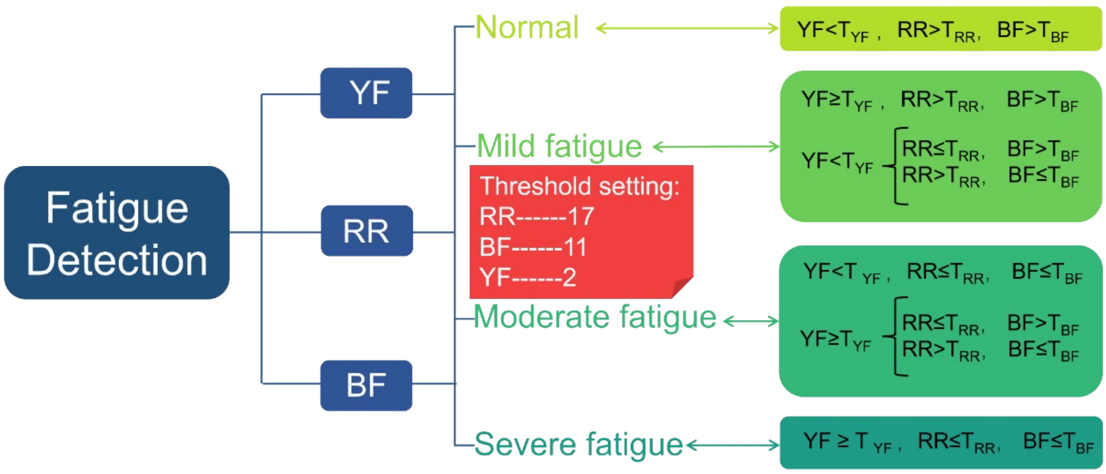


**Fig. S32** Flow chart of fatigue driving judgment.

| **Tester** | **Gender** | **Age** | **Weight(kg)** | **Height(cm)** |
| --- | --- | --- | --- | --- |
| Tester1 | Female | 22 | 54 | 155 |
| Tester2 | Female | 23 | 59 | 172 |
| Tester3 | Female | 24 | 50 | 160 |
| Tester4 | Male | 23 | 78 | 180 |
| Tester5 | Male | 24 | 70 | 180 |
| Tester6 | Male | 26 | 65 | 170 |

Table S1. Information of six volunteers for fatigue detection.

| | N_RR | N_BF | F_RR | F_BF |
|---|---|---|---|---|
| Group 1 | 23 | 18 | 13 | 8 |
| Group 2 | 20 | 15 | 12 | 7 |
| Group 3 | 22 | 14 | 15 | 9 |
| Group 4 | 21 | 15 | 14 | 7 |
| Group 5 | 23 | 13 | 16 | 10 |
| Group 6 | 23 | 12 | 12 | 8 |
| Group 7 | 21 | 18 | 12 | 7 |
| Group 8 | 22 | 17 | 13 | 8 |
| Group 9 | 20 | 16 | 16 | 8 |
| Group 10 | 21 | 16 | 14 | 7 |
| Group 11 | 23 | 18 | 13 | 9 |
| Group 12 | 23 | 17 | 15 | 10 |
| Group 13 | 24 | 19 | 16 | 7 |
| Group 14 | 25 | 20 | 14 | 6 |
| Group 15 | 23 | 20 | 16 | 8 |
| Group 16 | 26 | 18 | 15 | 9 |
| Group 17 | 23 | 19 | 16 | 10 |
| Group 18 | 23 | 17 | 16 | 9 |
| Group 19 | 24 | 16 | 15 | 8 |
| Group 20 | 23 | 15 | 14 | 6 |
| Group 21 | 24 | 13 | 12 | 7 |

| | | | | |
|---|---|---|---|---|
| Group 22 | 23 | 12 | 13 | 9 |
| Group 23 | 24 | 15 | 14 | 6 |
| Group 24 | 22 | 18 | 15 | 9 |
| Group 25 | 21 | 18 | 14 | 9 |
| Group 26 | 20 | 13 | 10 | 8 |
| Group 27 | 19 | 18 | 11 | 7 |
| Group 28 | 21 | 16 | 12 | 9 |
| Group 29 | 18 | 13 | 13 | 10 |
| Group 30 | 20 | 12 | 11 | 8 |

Table S2. Values of RR and BF under normal and fatigue conditions extracted from 30 groups of waveform data.

Supplemental references：


[1] H. Song, H. Wang, T. Gan, S. Shi, X. Zhou, Y. Zhang and S. Handschuh-Wang, *Adv. Mater. Technol.*, 2023, 2301483.

[2] X. Li, X. Xiao, C. Bai, M. Mayer, X. Cui, K. Lin, Y. Li, H. Zhang and J. Chen, *J. Mater. Chem. C*, 2022, **10**, 13789–13796.

[3] P. Yang, K. Liu, Q. Chen, X. Mo, Y. Zhou, S. Li, G. Feng and J. Zhou, *Angew. Chem., Int. Ed.*, 2016, **55**, 12050–12053.

[4] X. Li, J. Li, T. Wang, S. A. Khan, Z. Yuan, Y. Yin and H. Zhang, *ACS Appl. Mater. Interfaces*, 2022, **14**, 48743–48751.

[5] Y. Liu, S. Zhang, Y. Zhou, M. A. Buckingham, L. Aldous, P. C. Sherrell, G. G. Wallace, G. Ryder, S. Faisal, D. L. Officer, S. Beirne and J. Chen, *Advanced Energy Materials*, 2020, **10**, 2002539.